



Feasibility of an alternative method to estimate glenohumeral joint center from videogrammetry measurements and CT/MRI of patients

Ehsan Sarshari^{a,b}, Matteo Mancuso^c, Alexandre Terrier^b, Alain Farron^d, Philippe Mullhaupt^a and Dominique Pioletti^b

^aAutomatic Control Laboratory, Ecole Polytechnique Fédérale de Lausanne (EPFL), Lausanne, Switzerland; ^bLaboratory of Biomechanical Orthopedics, Ecole Polytechnique Fédérale de Lausanne (EPFL), Lausanne, Switzerland; ^cLaboratory of Movement Analysis and Measurement, Ecole Polytechnique Fédérale de Lausanne (EPFL), Lausanne, Switzerland; ^dService of Orthopaedic Surgery and Traumatology, Lausanne University Hospital and University of Lausanne (CHUV), Lausanne, Switzerland

ABSTRACT

Videogrammetry is commonly used to record upper limb motions. However, it cannot track the glenohumeral joint center (GH). GH is required to reconstruct upper limb motions. Therefore, it is often estimated by separately measuring scapular motions using scapular kinematics measurements devices (SKMD). Applications of SKMD are neither straightforward nor always noninvasive. Therefore, this work investigates the feasibility of an alternative method to estimate GH from videogrammetry using a CT/MRI image of subject's glenohumeral joint and without requiring SKMD. In order to evaluate the method's accuracy, its GH estimations were compared to reference GH trajectories. The method was also applied to estimate scapular configurations and reconstruct an abduction motion measured by videogrammetry. The accuracy of GH estimations were within 5 mm, and the reconstructed motion was in good agreement with reported *in vivo* measurements.

ARTICLE HISTORY

Received 25 March 2019
Accepted 8 August 2020

KEYWORDS

Upper limb kinematics; glenohumeral-joint center; videogrammetry; multi-segment optimization; scapular kinematics

1. Introduction

Videogrammetry tracks trajectories of skin-fixed markers placed on palpable bony landmarks (Winter 2009). It is not possible to palpate and measure GH using videogrammetry. However, GH is required to reconstruct upper-limb motions (Lu and O'Connor 1999; Roux et al. 2002).

Several methods have been developed to estimate GH, namely: formal (Woltring et al. 1985; Gamage and Lasenby 2002; Halvorsen 2003; Schwartz and Rozumalski 2005; Camomilla et al. 2006; Ehrig et al. 2006) and predictive methods (Meskers et al. 1997; Schmidt et al. 1999; Lloyd et al. 2000; Campbell et al. 2009). Formal methods estimate GH by finding either the closest point to all humerus instantaneous helical axes (Woltring et al. 1985; Schwartz and Rozumalski 2005; Camomilla et al. 2006; Ehrig et al. 2006) or the center of a sphere passing through humerus markers (Gamage and Lasenby 2002; Halvorsen 2003). Predictive methods estimate GH either through regressive equations between scapula markers and GH (Meskers et al. 1997; Lloyd et al. 2000; Campbell et al. 2009) or generic offsets from scapula markers

(Schmidt et al. 1999; Campbell et al. 2009). Formal methods estimate GH more accurately and are preferred over predictive methods whose accuracy drops significantly during arm motions (Ehrig et al. 2006; Campbell et al. 2009). The main limitation of formal methods is, however, their dependency on SKMD.

Due to soft tissue artifacts, only two landmarks—angulus acromialis (AA) and acromioclavicular (AC)—of the scapula can be practically tracked by videogrammetry (Matsui et al. 2006; Lempereur et al. 2010). SKMD is therefore used to measure scapular motions. Several SKMD have been proposed, including intracortical bone-fixed pins (Karduna et al. 2001), regressive equations (Högfors et al. 1991; De Groot and Brand 2001; Holzbaaur et al. 2005; Dickerson et al. 2007; Grewal and Dickerson 2013), scapula locator fixtures (McQuade and Smidt 1998; Prinold et al. 2011), and acromion markers-tree (van Andel et al. 2009). Applications of SKMD are, however, neither straightforward nor always non-invasive.

Therefore, this study aims at investigating the feasibility of an alternative method to estimate GH from videogrammetry using a CT/MRI of subject's glenohumeral joint and without requiring SKMD. Provided

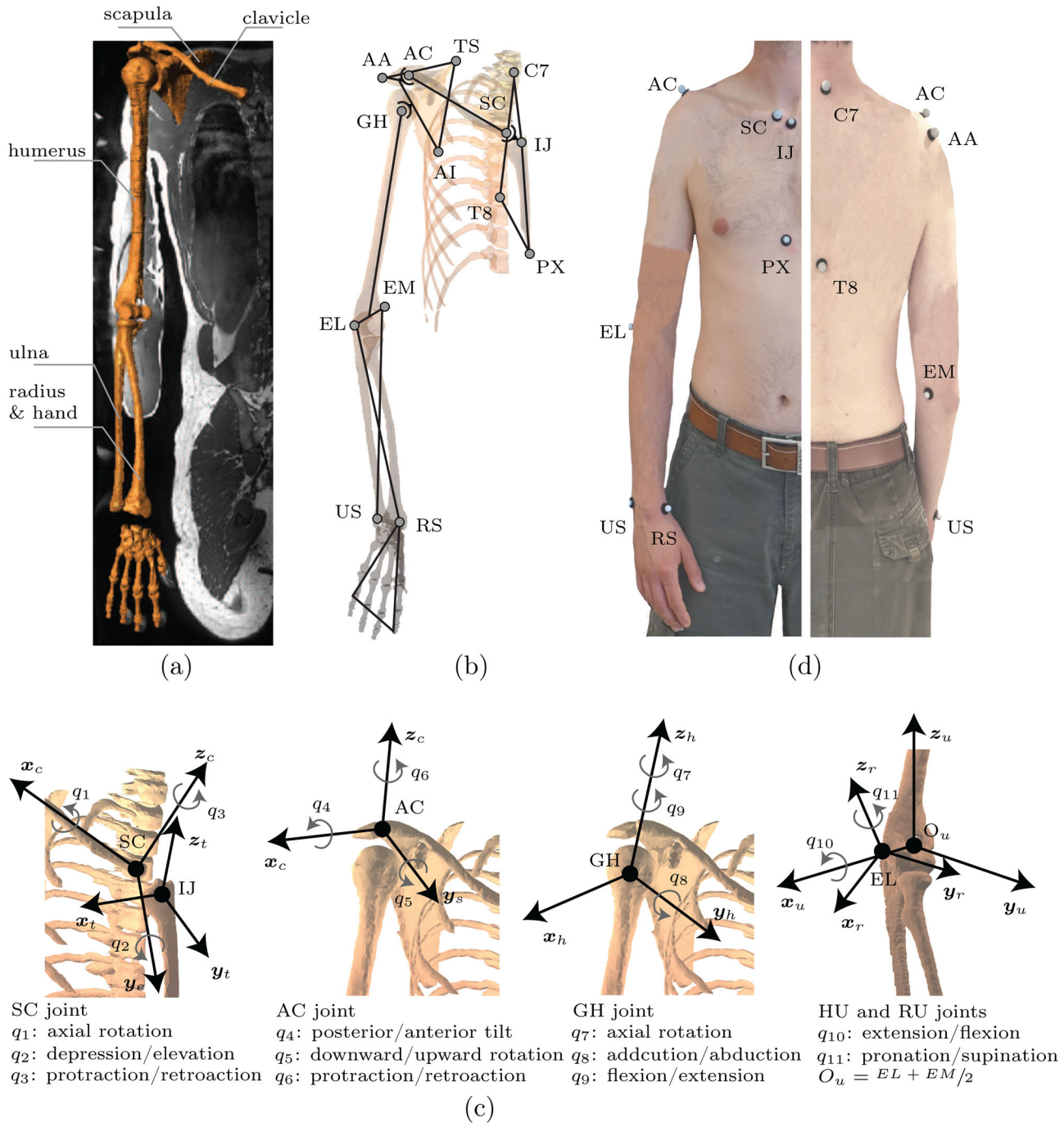


Figure 1. (a) Subject's MRI was used to develop the kinematic model. (b) Fourteen landmarks are considered. (c) Eleven generalized coordinates are considered ($q = [q_1 \dots q_{11}]^T$). (d) VICON videogrammetry is used to track eleven skin-fixed markers.

GH estimations, trigonum scapulae (TS) and angulus inferior (AI) of the scapula are consequently estimated defining the scapular configurations. The method's accuracy is evaluated by comparing its GH estimations to reference GH trajectories. The method is then applied to reconstruct an abduction motion measured by videogrammetry and compare the reconstructed motion to reported *in vivo* measurements.

2. Methods

2.1. Kinematic model

A kinematic model of the upper limb is developed from MRI scans (T1-weighted sequences, 3-T, 0.9 mm isotropic spatial resolution) of the hemi-thorax of a healthy male subject (29 year, 186 cm, 85.5 kg) (Figure 1(a)). It consists of six rigid bodies: thorax, clavicle,

scapula, humerus, ulna, and radius (rigidly tied with hand). It has five joints, including three ball-and-socket joints for sternoclavicular (SC), acromioclavicular (AC), and glenohumeral (GH) joints and two hinge joints for humeroulnar (HU) and radioulnar (RU) joints (Figure 1(b,c)). Two holonomic constraints restrict TS and AI to glide over the ribcage. This results in nine degrees of freedom. Fourteen bony landmarks are identified from the MRI scans to define bone-fixed frames and joint coordinates following ISB recommendations (International Society of Biomechanics 2005). The landmarks are: incisura jugularis (IJ), processus xiphoideus (PX), 7th cervical vertebra (C7), 8th thoracic vertebra (T8), SC, AC, AA, TS, AI, GH, humerus medial epicondyle (EM), humerus lateral epicondyle (EL), radial styloid (RS), and ulnar styloid (US). Given that the GH is not a bony landmark, its position is defined as the center of a sphere fitting the glenoid fossa (Veeger 2000). To this end, a MATLAB (The MathWorks, Natick, MA, USA) routine (Terrier et al. 2014) is used to fit a sphere on the fossa surface obtained by segmentation of MRI in Amira (FEI Visualization Sciences Group, Bordeaux, France). The thorax is the inertial frame. Eleven generalized coordinates ($\mathbf{q} = [q_1 \dots q_{11}]^T$) are considered to uniquely define each joint configuration. The forward kinematic map (ξ) of the kinematic model defines the inertial coordinates of the j th landmark (\mathbf{x}_j) for given joint configurations

$$\begin{aligned} \xi : C_s \subset R^{11} &\mapsto W_s \subset R^3 \\ \xi(\mathbf{q}(t)) &= \mathbf{x}_j(t), \quad j = \{C7, \dots, RS\}_{1 \times 14} \\ \Phi_{TS}(\mathbf{q}(t)) &= 0 \\ \Phi_{AI}(\mathbf{q}(t)) &= 0 \end{aligned} \quad (1)$$

where C_s and W_s are coordinate and work spaces (Siciliano and Khatib 2008). The holonomic constraints ($\Phi_{TS} = 0$ and $\Phi_{AI} = 0$) represent kinematic relationships between the scapula and the thorax (Equation 2). The constraints restrict TS and AI to always lie on two different ellipsoids approximating the ribcage and the underlying soft tissues of each one of TS and AI

$$\begin{aligned} \Phi_{TS}(\mathbf{q}(t)) &= ({}_t\mathbf{TS}(t) - {}_t\mathbf{e}_0)^T E_{TS} ({}_t\mathbf{TS}(t) - {}_t\mathbf{e}_0) - 1 = 0 \\ \Phi_{AI}(\mathbf{q}(t)) &= ({}_t\mathbf{AI}(t) - {}_t\mathbf{e}_0)^T E_{AI} ({}_t\mathbf{AI}(t) - {}_t\mathbf{e}_0) - 1 = 0 \end{aligned} \quad (2)$$

where the left-hand side subscript t denotes that the landmarks are in the thorax frame. The centers of the two ellipsoids coincide and are at ${}_t\mathbf{e}_0$. A single ellipsoid centered at ${}_t\mathbf{e}_0$ is first fitted to the ribcage. Then, starting from this ellipsoid, adjustments are made to fit one ellipsoid to AI and another ellipsoid to TS.

The ellipsoids including TS and AI have matrices E_{TS} and E_{AI} , respectively (Levin 1979).

2.2. Estimation of GH

Ball-and-socket approximation of the glenohumeral joint implies that GH is a point shared between the scapula and the humerus (Figure 2). Therefore, its positions as a point either on the scapula or the humerus should result in the same point in the thorax frame (${}_t\mathbf{GH}$). This can be concisely written as

$$\underbrace{{}_h^t R(\alpha) \quad {}_h\mathbf{GH} + {}_t\mathbf{EM}}_{\text{{}_tGH as a point on humerus}} = \underbrace{{}_s^t R(\beta) \quad {}_s\mathbf{GH} + {}_t\mathbf{AC}}_{\text{{}_tGH as a point on scapula}} \quad (3)$$

where ${}_h^t R(\alpha)$ and ${}_s^t R(\beta)$ are the rotation matrices from the humerus frame and the scapular frame to the thorax frame, respectively. The rotation matrices ${}_h^t R(\alpha)$ and ${}_s^t R(\beta)$ are defined in Equation (4) using Rodrigues' rotation formula (Baruh 1999). The left-hand side subscripts h and s specify that the landmarks are in the humerus and the scapular frames, respectively. Constants ${}_h\mathbf{GH}$ and ${}_s\mathbf{GH}$ are obtained from the subject's CT/MRI. From a CT of the subject to be studied ${}_{CT}\mathbf{GH}$, ${}_{CT}\mathbf{EM}$, ${}_{CT}\mathbf{EL}$ that are the landmarks in the CT or MRI coordinate system can be obtained for a single arm configuration. Then, ${}_h\mathbf{GH}$ is defined as ${}_h\mathbf{GH} = {}_{CT}^h R \quad {}_{CT}\mathbf{GH}$. The rotation matrix ${}_{CT}^h R$ from the CT or MRI coordinate system to the humeral coordinate system is obtained following the ISB recommendations (International Society of Biomechanics 2005). Similarly, ${}_s\mathbf{GH}$ is obtained as ${}_s\mathbf{GH} = {}_{CT}^s R \quad ({}_{CT}\mathbf{GH} - {}_{CT}\mathbf{AC})$. The rotation matrix ${}_{CT}^s R$ from the CT or MRI coordinate system to the scapular coordinate system is obtained following the ISB recommendations.

$$\begin{aligned} {}_h^t R(\alpha) &= \mathbf{d}_h \mathbf{d}_h^T + \cos \alpha (I - \mathbf{d}_h \mathbf{d}_h^T) + \sin \alpha [\mathbf{d}_h] \\ {}_s^t R(\beta) &= \mathbf{d}_s \mathbf{d}_s^T + \cos \beta (I - \mathbf{d}_s \mathbf{d}_s^T) + \sin \beta [\mathbf{d}_s] \end{aligned} \quad (4)$$

where $\mathbf{d}_h = {}_t\mathbf{EM} - {}_t\mathbf{EL}$ and $\mathbf{d}_s = {}_t\mathbf{AC} - {}_t\mathbf{AA}$, and α and β are unknown rotation angles of the humerus and the scapula around \mathbf{d}_h and \mathbf{d}_s . The cross product matrices of \mathbf{d}_h and \mathbf{d}_s are denoted by $[\mathbf{d}_h]$ and $[\mathbf{d}_s]$, respectively.

Equation (3) can be solved for α and β for each frame of measurements using nonlinear root-search methods (e.g. Matlab `fminsearch`). The resulting α and β provide two estimations for GH in thorax frame (${}_t\mathbf{GH}$). Given that the measured positions of AC, AA, EM, and EL are subject to soft-tissue artifacts, the resulting two estimations of ${}_t\mathbf{GH}$ might come apart. Therefore, the following optimization is set to minimize the distance between the resulting

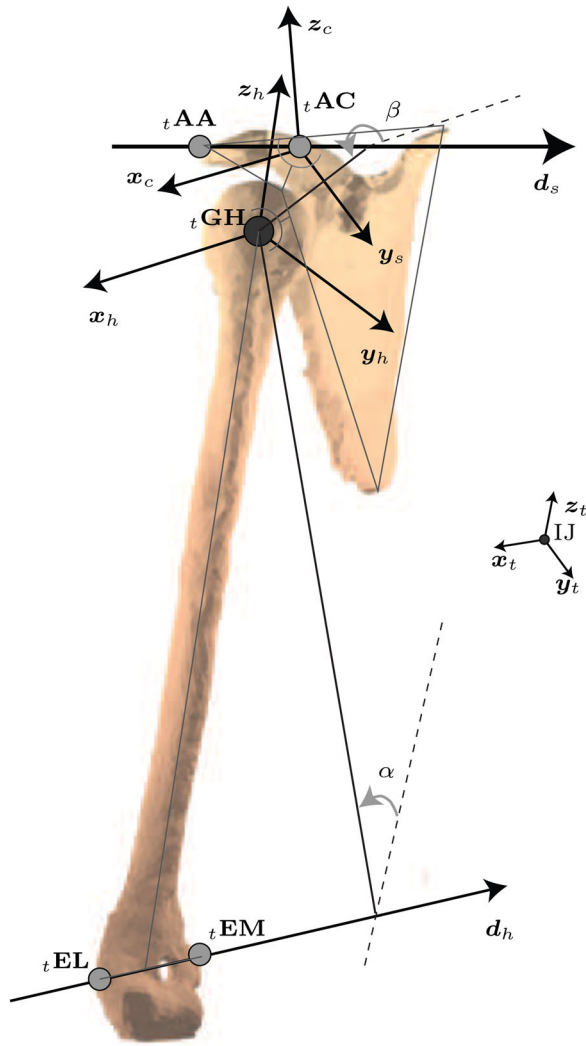


Figure 2. GH belongs to both humerus and scapula. The estimated ${}^t\text{GH}$ lies on the intersection of two line segments in planes perpendicular to \mathbf{d}_h and \mathbf{d}_s . These two line segments form two angles (α and β) with respect to reference axes that can be found by solving Equation (3).

two estimations by compensating the effects of soft-tissue artifacts on EM and EL

$$\begin{aligned} \min_{\boldsymbol{\mu}} \quad & ({}^t\text{GH}_{e_h}(\boldsymbol{\mu}) - {}^t\text{GH}_{e_s}(\boldsymbol{\mu}))^2 \\ \text{s.t.} \quad & |\boldsymbol{\mu}| \leq C \end{aligned} \quad (5)$$

where ${}^t\text{GH}_{e_h}$ and ${}^t\text{GH}_{e_s}$ are the resulting estimations obtained through the humerus and the scapular frames, respectively. The decision variable $\boldsymbol{\mu}$ is a 3×1 vector added to \mathbf{d}_h to compensate soft-tissue artifacts. It is bounded by C to vary according to reported values for EM and EL soft-tissue artifacts [$C=3$ cm (Klopčar and Lenarčič 2006)].

The estimated GH together with the measured AC and AA provide three points on the scapula. Therefore, TS and AI are readily estimated, given that

they also belong to the same bone segment. The resulting GH, TS, and AI estimations are used in Section 2.3 to reconstruct the shoulder kinematics including scapular configuration.

It is worth noting that Equation (3) has an intuitive geometrical interpretation. It estimates GH by intersecting four spheres centered at AC, AA, EM, and EL. Their radii can be defined from a single CT/MRI scan of the glenohumeral joint of the subject to be studied. This intersection can be defined using the intersection theory of quadric surfaces (Levin 1979).

2.3. Multi-segment optimization

Multi-segment optimization finds joint angles (\mathbf{q}_i) for each frame of measurement (i) such that the overall distance between the measured markers (\mathbf{x}_{e_j}) and their associated landmarks (\mathbf{x}_{m_j}) is minimized, while satisfying the forward kinematics map (Equation 6). Estimations of GH, TS, and AI are considered through their missing measured trajectories.

$$\begin{aligned} \min_{\mathbf{q}_i} \quad & \sum_j (\mathbf{x}_{m_j,i}(\mathbf{q}_i) - \mathbf{x}_{e_j,i})^T W (\mathbf{x}_{m_j,i}(\mathbf{q}_i) - \mathbf{x}_{e_j,i}) \\ \text{s.t.} \quad & \Phi_{\text{TS}}(\mathbf{q}_i) = 0 \\ & \Phi_{\text{AI}}(\mathbf{q}_i) = 0 \end{aligned} \quad (6)$$

where $j = \{C7, \dots, \text{RS}\}_{1 \times 14}$, and W is a positive-definite weighting matrix that can be used to account for different amounts of soft-tissue artifacts occur at each marker (Begon et al. 2015). For simplicity, W is set to the identity matrix here. This optimization is a nonlinear programming problem (Boyd and Vandenberghe 2004) that can be solved using iterative methods (e.g. Matlab fmincon).

2.4. Accuracy

A numerical method (Ingram et al. 2016)—called minimal coordinate approach—is used to virtually generate trajectories for all fourteen model's landmarks during forward flexion. The minimal coordinate approach is indeed the only available method that can plan the upper limb motions from a limited amount of measurement data (Ingram et al. 2016). In the minimal coordinate approach, the shoulder girdle contact constraint is replaced by a novel parallel mechanism that results in a minimal set of generalized coordinates. The resulting minimal coordinates are independent and considerably simplify motion planning. The accuracy of the minimal coordinate approach has been already investigated in (Ingram 2015) against *in vivo* measurements of El Habachi et al. (2015). An arm motion from the arm neutral

position to 150° flexion is simulated using the minimal coordinate approach. To this end, the scapular minimal coordinates corresponding to the beginning and the end of the motion are chosen as per Ingram (2015), such that the model bony landmarks match the bony landmarks reported by El Habachi et al. (2015), only for the beginning and the end of the motion. Until 30° of arm elevation, the scapular minimal coordinates are maintained at their initial values and thereafter are linearly changed with time to reach the end-motion values. The definition of the arm minimal coordinates are trivial using a linear function of time until 150° of flexion. Eventually, GH of the virtually generated trajectories is considered as the reference GH (${}_t\mathbf{GH}_r$). Soft-tissue artifacts are numerically produced and added to the trajectories. Soft-tissue artifacts are defined according to Cheze et al. (1995), Taylor et al. (2005) as $a \sin(\omega t + \phi)$, where a lies between 1 cm and 3 cm, and ω and ϕ are smaller than 4 Hz and 2π rad, respectively. The resulting trajectories are considered as pseudo-measurements. The method is used to estimate GH from the pseudo-measurements.

The accuracy results are presented in terms of the distance d between estimated GH (${}_t\mathbf{GH}_e$) and ${}_t\mathbf{GH}_r$ for each frame of data.

2.5. Motion reconstruction from videogrammetry

Eleven bony landmarks are palpated using skin-fixed markers on the same subject, including IJ, PX, C7, T8, SC, AC, AA, EM, EL, RS, and US (Figure 1(d)). The marker trajectories are recorded for 10 trials using an 8-camera VICON videogrammetry at 100 Hz, while the subject is performing an abduction motion in the scapular plane with a fully extended forearm. The recorded data of each trial is low-pass filtered (Winter 2009). Then, the means and the standard deviations (σ) of the filtered trajectories for the 10 trials are obtained.

The method is used to estimate GH and consequently TS and AI. Then, multi-segment optimization is used to reconstruct the motion in terms of the joint angles. Sensitivity of the joint angles ($\mathbf{q}(\Delta\mathbf{x})$) to marker variations around their means ($\Delta\mathbf{x}$) are also approximated by a first-order approximation (Equation 7) (Fiacco 1976)

$$\mathbf{q}(\Delta\mathbf{x}) = \mathbf{q}^* + M^{-1}N\Delta\mathbf{x} + O(|\Delta\mathbf{x}|) \quad (7)$$

where \mathbf{q}^* is solution of the multi-segment optimization associated with measurement means. The matrices M and N are defined as follows

$$M = \begin{bmatrix} \nabla^2 L & \nabla\Phi_{TS} & \nabla\Phi_{AI} \\ \nabla\Phi_{TS} & 0 & 0 \\ \nabla\Phi_{AI} & 0 & 0 \end{bmatrix},$$

$$N = \left[-\frac{\partial}{\partial\Delta\mathbf{x}}(\nabla L) \quad -\frac{\partial\Phi_{TS}}{\partial\Delta\mathbf{x}} \quad -\frac{\partial\Phi_{AI}}{\partial\Delta\mathbf{x}} \right]^T \quad (8)$$

where L is the Lagrangian of the multi-segment optimization (Equation 6).

The results consist of eleven joints angles, including axial rotation, depression/elevation, protraction/retraction of SC, posterior/anterior tilt, downward/upward rotation, protraction/retroaction of AC, axial rotation, adduction/abduction, flexion/extension of GH, extension/flexion of HU, and pronation/supination of RU joints. Joint angles are presented in the thorax frame along the arm abduction angle, except for HU and RU joints, which are given with respect to their proximal joints. Angles sensitivities to $\pm 1\sigma$ marker variations are also illustrated.

3. Results

3.1. Accuracy

The distance d was <1 mm until 20% of arm flexion and reached 5 mm at 60% of the movement (Figure 3).

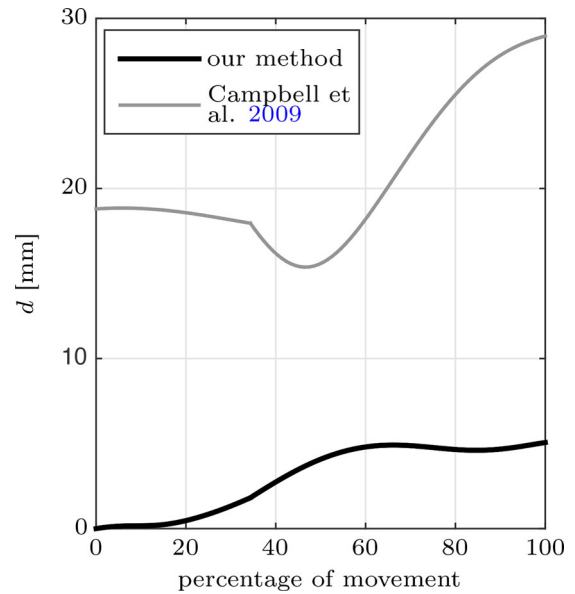


Figure 3. Method accuracy, distance d of the estimated GH to its reference position during arm flexion. The model developed in Campbell et al. (2009) was directly applied in this study to the same pseudo-measurements, and the corresponding results were presented.

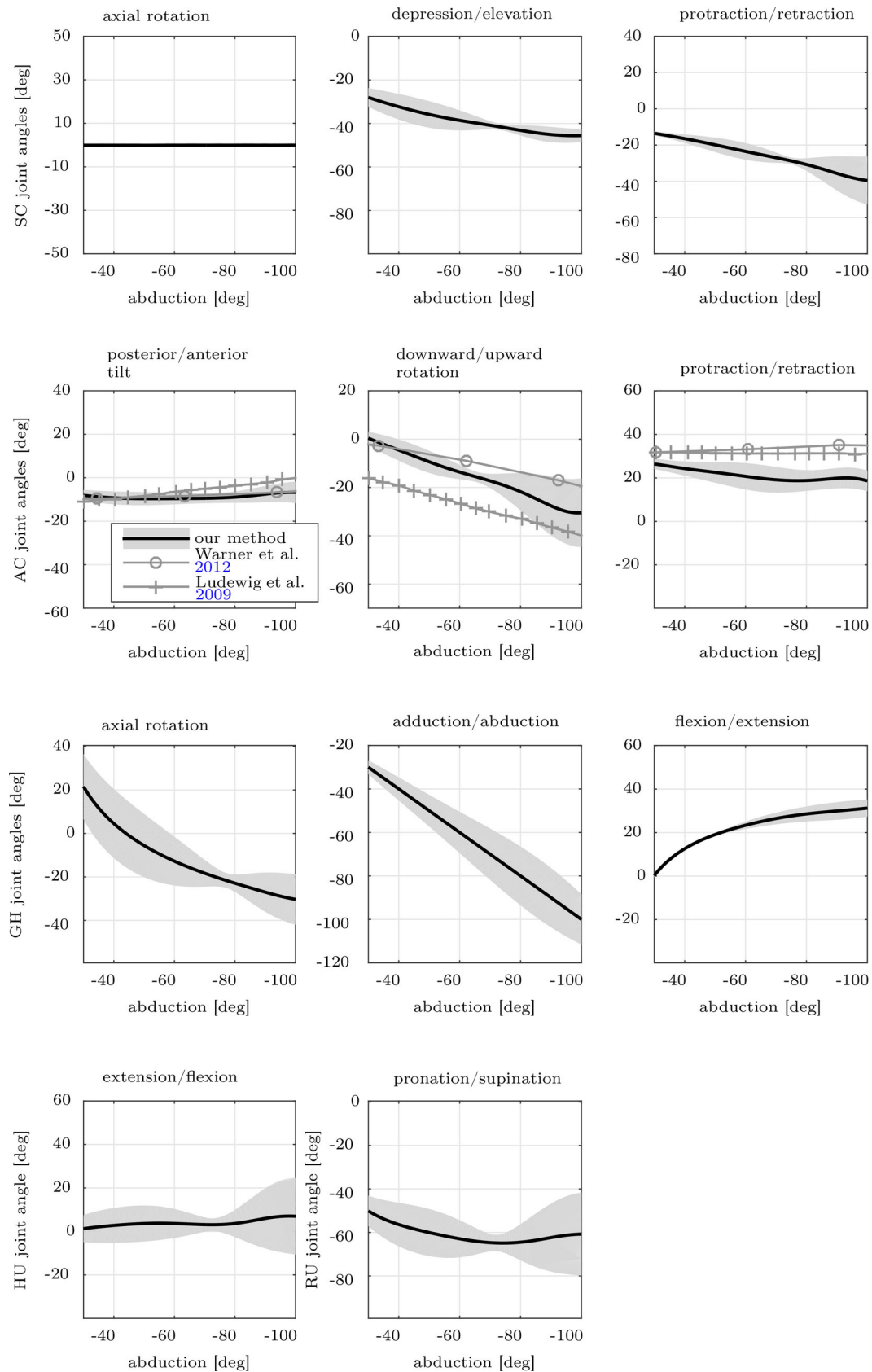


Figure 4. Motion reconstruction, the measured abduction motion was reconstructed in terms of 11 joint angles. The angle sensitivities to $\pm 1\sigma$ landmark variations were presented as the shaded area. The AC joint angles measured *in vivo* by Ludewig et al. (2009), Warner et al. (2012) were also presented, given the importance of the scapular kinematics.

3.2. Motion reconstruction from videogrammetry

The clavicular elevation and retraction increased by 16° and 26° during the arm elevation, despite its axial rotation, and were equally (about 13°) affected by landmark variations (Figure 4).

The scapular posterior tilt increased by 5° from an anteriorly tilted configuration. The scapular upward rotation increased from a neutral position to 30° . The scapular protraction decreased by 7° . The landmark variations affected posterior/anterior tilt by 5° , downward/upward rotation by 13° , and protraction/retraction by 6° .

The humerus rotated externally by 49° from an internally orientated position. Abduction increased by 68° , and flexion increased by 30° . Axial rotation and adduction/abduction were almost 250% more sensitive to landmarks variations than flexion/extension angle.

The forearm flexed 6° from full extension, and RU supination increased by 9° (palm of the hand faced anteriorly). Compared to other joint angles, the forearm illustrated the highest sensitivities to landmarks variations: (17° and 22° for HU and RU joints, respectively).

4. Discussion

The aim of this study was to develop a method to estimate GH from videogrammetry using a CT/MRI of subject's glenohumeral joint and without requiring SKMD. The method accuracy was verified, and the method was applied to reconstruct a videogrammetry-based measured motion.

The accuracy decreased towards the end of the motion that could be associated with the increase in simulated soft-tissue artifacts. The increasing trend considered for soft-tissue artifacts was consistent with previous *in vivo* observations (Cheze et al. 1995; Taylor et al. 2005). Compared to the application of a reported predictive method (Campbell et al. 2009) on the same pseudo-measurements, GH estimation was improved around 85% with our method. The choice of the predictive method (Campbell et al. 2009), among the available predictive methods in the literature, could be justified by the following main reasons. First, contrary to most of the predictive methods (Meskers et al. 1997; International Society of Biomechanics 2005), it did not require trajectories of TS or AI. Trajectories of TS and AI could only be either measured using SKMD or estimated based on GH trajectories. Second, it was indeed among the few predictive methods whose accuracy and inter-individual reliability have been assessed against other

established predictive methods (Meskers et al. 1997; Schmidt et al. 1999; Lloyd et al. 2000; International Society of Biomechanics 2005), as well as *in vivo* GH measurements.

Application of the method to videogrammetry measurements followed by the multi-segment optimization provided joint angles that were consistent with reported *in vivo* (Ludewig et al. 2009; Warner et al. 2012) and numerical studies (Seth et al. 2016; Naaim et al. 2017).

The clavicular axial rotation was overlooked in our motion reconstruction, whereas several *in vivo* studies reported 0° to 30° variations (Sahara et al. 2007; Ludewig et al. 2009). The clavicular axial rotation could be enforced using an extra constraint on q_1 in Equation (6) (van der Helm and Pronk 1995). However, given few weak muscles attached to the clavicle, underestimating its axial rotation has only negligible effects on musculoskeletal model outcomes (Prinold et al. 2013).

AC joint angles were in good agreement with *in vivo* measurements (Ludewig et al. 2009; Warner et al. 2012). Normalized root-mean-square error (NRMSE) (Matlab Documentation 2012) between the estimated scapular posterior/anterior tilt and the measurements of Warner et al. (2012) and Ludewig et al. (2009) were 0.99 and 0.91, respectively. The NRMSE between the estimated scapular downward/upward rotation and the measurements was consistent with the results of Warner et al. (2012) (NRMSE above 0.77). The zero downward rotation estimated by our model placed the scapula in a rest position for the beginning of motion and was commonly reported (MacLean et al. 2014; Naaim et al. 2017), although the angle reported in Ludewig et al. (2009) was -16° . The estimated scapular protraction/retraction was consistent with both *in vivo* measurements of Ludewig et al. (2009), Warner et al. (2012) (NRMSE above 0.81).

The forearm joint angles had the highest sensitivities to variations in marker trajectories. This could be explained by propagation of errors introduced through proximal bone segments. The sensitivity analysis investigated the sensitivity of the resulting joint angles to the recorded variations in marker trajectories. Although this provided valuable information about the reliability of the resulting joint angles, a more detailed sensitivity study would be required to investigate influences of positioning each individual marker. With such a detailed sensitivity study, special attention could be paid to capture more robustly the trajectories of the influential markers.

The effects of soft-tissue artifacts on GH estimations were compensated by an optimization. The optimization accounted for merely EM and EL soft-tissue artifacts, since AC and AA were subject to relatively negligible amount of soft-tissue artifacts (Blache et al. 2017; Duprey et al. 2017; Naaim et al. 2017). In addition, from a mathematical point of view, it would be possible to introduce a second decision variable into the optimization for AC and AA soft-tissue artifacts. However, this would result in an indeterminate optimization with infinite solutions. In order to obtain a unique solution, complementary information on the ratio of EM-EL to AC-AA soft-tissue artifacts would be required. Application of a marker cluster attached to the humerus could potentially reduce the amount of soft-tissue artifacts, requiring less correction from the optimization.

A major limitation of this study was that only one subject was recorded. A larger number of subjects would allow a better evaluation of the method, particularly its performance in dealing with inter-individual differences. Nevertheless, the method already took into account, to a certain extent, inter-individual differences. Indeed, it required patient-specific data from a CT/MRI scan of the subject's glenohumeral joint as explained in Section 2.2. Another limitation was the dependency of the method on subject's CT/MRI. The CT/MRI is often performed during subjects' routine clinical examinations. Therefore, it would not widely affect practical applications of the method for subject-specific modeling. Another potential limitation of the method was due to the high error sensitivity of the direction connecting EL and EM and/or AC and AA, given the short distances between them. Therefore, special care was taken in placing the markers on these bony landmarks. In addition, an additional marker on the Capitulum could help in compensating the error in direction connecting EL and EM.

The resulting GH estimations and scapular kinematics were compared to those of a commonly used predictive method and *in vivo* measurements, respectively. These partially confirmed the feasibility of the present method as an alternative approach to estimate the GH and the scapular kinematics without SKMD. Indeed, direct comparisons of the method estimations with measurements from SKMD such as scapula locator and acromion cluster could enrich the confidence into the method estimations.

In conclusion, the method provided estimations for GH, TS, and AI with sufficient accuracy using a CT/MRI scan of subject's glenohumeral joint and without requiring SKMD. Provided GH, TS, and AI

estimations, a videogrammetry-based measured motion was reconstructed using multi-segment optimization which resulted in scapula configurations that were in good agreement with reported *in vivo* measurements. The developed method could be used to retrospectively study kinematics of patients using a scaled-generic shoulder musculoskeletal model. A generic motion data could be scaled to each patient whose CT/MRI is available as a part of a routine clinical examination.

Funding

This project was supported by the Swiss National Science Foundation [143704].

Disclosure statement

No potential conflict of interest was reported by the authors.

References

- Baruh H. 1999. Analytical dynamics. Boston: WCB/McGraw-Hill.
- Begon M, Dal Maso F, Arndt A, Monnet T. 2015. Can optimal marker weightings improve thoracohumeral kinematics accuracy? *J Biomech.* 48(10):2019–2025.
- Blache Y, Dumas R, Lundberg A, Begon M. 2017. Main component of soft tissue artifact of the upper-limbs with respect to different functional, daily life and sports movements. *J Biomech.* 62:39–46.
- Boyd S, Vandenberghe L. 2004. Convex optimization. Cambridge: Cambridge University Press.
- Camomilla V, Cereatti A, Vannozzi G, Cappozzo A. 2006. An optimized protocol for hip joint centre determination using the functional method. *J Biomech.* 39(6): 1096–1106.
- Campbell A, Lloyd D, Alderson J, Elliott B. 2009. MRI development and validation of two new predictive methods of glenohumeral joint centre location identification and comparison with established techniques. *J Biomech.* 42(10):1527–1532.
- Cheze L, Fregly B, Dimnet J. 1995. A solidification procedure to facilitate kinematic analyses based on video system data. *J Biomech.* 28(7):879–884.
- De Groot J, Brand R. 2001. A three-dimensional regression model of the shoulder rhythm. *Clin Biomech (Bristol, Avon).* 16(9):735–743.
- de Groot JH, Valstar ER, Arwert HJ. 1998. Velocity effects on the scapulo-humeral rhythm. *Clin Biomech (Bristol, Avon).* 13(8):593–602.
- Dickerson CR, Chaffin DB, Hughes RE. 2007. A mathematical musculoskeletal shoulder model for proactive ergonomic analysis. *Comput Methods Biomech Biomed Eng.* 10(6):389–400.
- Duprey S, Naaim A, Moissenet F, Begon M, Chèze L. 2017. Kinematic models of the upper limb joints for multibody

- kinematics optimisation: an overview. *J Biomech.* 62: 87–94.
- Ehrig RM, Taylor WR, Duda GN, Heller MO. 2006. A survey of formal methods for determining the centre of rotation of ball joints. *J Biomech.* 39(15):2798–2809.
- El Habachi A, Duprey S, Cheze L, Dumas R. 2015. A parallel mechanism of the shoulder—application to multi-body optimisation. *Multibody Syst Dyn.* 33(4):439–451.
- Fiacco AV. 1976. Sensitivity analysis for nonlinear programming using penalty methods. *Math Program.* 10(1): 287–311.
- Gamage SSHU, Lasenby J. 2002. New least squares solutions for estimating the average centre of rotation and the axis of rotation. *J Biomech.* 35(1):87–93.
- Grewal T-J, Dickerson CR. 2013. A novel three-dimensional shoulder rhythm definition that includes overhead and axially rotated humeral postures. *J Biomech.* 46(3): 608–611.
- Halvorsen K. 2003. Bias compensated least squares estimate of the center of rotation. *J Biomech.* 36(7):999–1008.
- Högfors C, Peterson B, Sigholm G, Herberts P. 1991. Biomechanical model of the human shoulder joint—ii. the shoulder rhythm. *J Biomech.* 24(8):699–709.
- Holzbaier KR, Murray WM, Delp SL. 2005. A model of the upper extremity for simulating musculoskeletal surgery and analyzing neuromuscular control. *Ann Biomed Eng.* 33(6):829–840.
- Ingram D. 2015. Musculoskeletal model of the human shoulder for joint force estimation. Ph.D. Thesis, Ecole Polytechnique Fédérale de Lausanne, DOI: [10.5075/epfl-thesis-6497](https://doi.org/10.5075/epfl-thesis-6497).
- Ingram D, Engelhardt C, Farron A, Terrier A, Müllhaupt P. 2016. Modelling of the human shoulder as a parallel mechanism without constraints. *Mech Mach Theory.* 100:120–137.
- Karduna AR, McClure PW, Michener LA, Sennett B. 2001. Dynamic measurements of three-dimensional scapular kinematics: a validation study. *J Biomech Eng.* 123(2): 184–190.
- Klopčar N, Lenarčič J. 2006. Bilateral and unilateral shoulder girdle kinematics during humeral elevation. *Clin Biomech.* 21:S20–S26.
- Lempereur M, Brochard S, Burdin V, Rémy-Néris O. 2010. Difference between palpation and optoelectronics recording of scapular motion. *Comput Methods Biomed Eng.* 13(1):49–57.
- Levin JZ. 1979. Mathematical models for determining the intersections of quadric surfaces. *Comput Graph Image Process.* 11(1):73–87.
- Lloyd D, Alderson J, Elliott B. 2000. An upper limb kinematic model for the examination of cricket bowling: a case study of Mutiah muralitharan. *J Sports Sci.* 18(12): 975–982.
- Lu TW, O'Connor JJ. 1999. Bone position estimation from skin marker co-ordinates using global optimisation with joint constraints. *J Biomech.* 32(2):129–134.
- Ludewig PM, Phadke V, Braman JP, Hassett DR, Cieminski CJ, LaPrade RF. 2009. Motion of the shoulder complex during multiplanar humeral elevation. *J Bone Joint Surg Am.* 91(2):378–389.
- MacLean KF, Chopp JN, Grewal T-J, Picco BR, Dickerson CR. 2014. Three-dimensional comparison of static and dynamic scapular motion tracking techniques. *J Electromyogr Kinesiol.* 24(1):65–71.
- Matlab Documentation. 2012. Goodness of fit between test and reference data. URL <https://ch.mathworks.com/help/ident/ref/goodnessoffit.html>.
- Matsui K, Shimada K, Andrew PD. 2006. Deviation of skin marker from bone target during movement of the scapula. *J Orthop Sci.* 11(2):180–184.
- McQuade KJ, Smidt GL. 1998. Dynamic scapulohumeral rhythm: the effects of external resistance during elevation of the arm in the scapular plane. *J Orthop Sports Phys Ther.* 27(2):125–133.
- Meskers C, Van der Helm FC, Rozendaal L, Rosing P. 1997. In vivo estimation of the glenohumeral joint rotation center from scapular bony landmarks by linear regression. *J Biomech.* 31(1):93–96.
- Naaim A, Moissenet F, Duprey S, Begon M, Cheze L. 2017. Effect of various upper limb multibody models on soft tissue artefact correction: a case study. *J Biomech.* 62: 102–109.
- Prinold JA, Masjedi M, Johnson GR, Bull AM. 2013. Musculoskeletal shoulder models: a technical review and proposals for research foci. *Proc Inst Mech Eng H.* 227(10):1041–1057.
- Prinold JA, Shaheen AF, Bull AM. 2011. Skin-fixed scapula trackers: a comparison of two dynamic methods across a range of calibration positions. *J Biomech.* 44(10): 2004–2007.
- Roux E, Bouilland S, Godillon-Maquinghen A-P, Bouttens D. 2002. Evaluation of the global optimisation method within the upper limb kinematics analysis. *J Biomech.* 35(9):1279–1283.
- Sahara W, Sugamoto K, Murai M, Tanaka H, Yoshikawa H. 2007. The three-dimensional motions of glenohumeral joint under semi-loaded condition during arm abduction using vertically open mri. *Clin Biomech (Bristol, Avon).* 22 (3):304–312.
- Schmidt R, Disselhorst-Klug C, Silny J, Rau G. 1999. A marker-based measurement procedure for unconstrained wrist and elbow motions. *J Biomech.* 32(6):615–621.
- Schwartz MH, Rozumalski A. 2005. A new method for estimating joint parameters from motion data. *J Biomech.* 38(1):107–116.
- Seth A, Matias R, Veloso AP, Delp SL. 2016. A biomechanical model of the scapulothoracic joint to accurately capture scapular kinematics during shoulder movements. *PLoS One.* 11(1):e0141028.
- Siciliano B, Khatib O. 2008. Springer handbook of robotics. Berlin: Springer Science & Business Media.
- Taylor WR, Ehrig RM, Duda GN, Schell H, Seebeck P, Heller MO. 2005. On the influence of soft tissue coverage in the determination of bone kinematics using skin markers. *J Orthop Res.* 23(4):726–734.
- Terrier A, Ston J, Larrea X, Farron A. 2014. Measurements of three-dimensional glenoid erosion when planning the prosthetic replacement of osteoarthritic shoulders. *Bone Joint J.* 96-B(4):513–518.
- van Andel C, van Hutten K, Eversdijk M, Veeger D, Harlaar J. 2009. Recording scapular motion using an acromion marker cluster. *Gait Posture.* 29(1):123–128.

- van der Helm FC, Pronk GM. 1995. Three-dimensional recording and description of motions of the shoulder mechanism. *J Biomech Eng.* 117(1):27–40.
- Veeger H. 2000. The position of the rotation center of the glenohumeral joint. *J Biomech.* 33(12):1711–1715.
- Warner M, Chappell P, Stokes M. 2012. Measuring scapular kinematics during arm lowering using the acromion marker cluster. *Hum Mov Sci.* 31(2): 386–396.
- Winter DA. 2009. *Biomechanics and motor control of human movement.* New York: John Wiley & Sons.
- Woltring H, Huiskes R, De Lange A, Veldpaus F. 1985. Finite centroid and helical axis estimation from noisy landmark measurements in the study of human joint kinematics. *J Biomech.* 18(5):379–389.
- Wu G, van der Helm FCT, Veeger HEJD, Makhsous M, Van Roy P, Anglin C, Nagels J, Karduna AR, McQuade K, Wang X, International Society of Biomechanics, et al. 2005. Is b recommendation on definitions of joint coordinate systems of various joints for the reporting of human joint motion-Part II: shoulder, elbow, wrist and hand. *J Biomech.* 38(5):981–992.